A THESIS FOR THE DEGREE OF MASTER OF SCIENCE

Crystal structure and branching mechanism of GH57-type glycogen branching enzyme from *Pyrococcus horikoshii*

Pyrococcus horikoshii 유래 GBE 의
결정 구조와 글리코젠의 가지 형성 기전의 규명

February, 2017

Soo Hui Na

Department of Agricultural Biotechnology
College of Agriculture and Life Sciences
Seoul National University

석사학위논문

Crystal structure of GH57-type glycogen branching enzyme from *Pyrococcus horikoshii*

지도교수 하 남 출

이 논문을 석사학위논문으로 제출함

2017 년 2 월

서울대학교 대학원

농생명공학부

나 수 휘

나수휘의 석사학위논문을 인준함

2017 년 2 월

위원장 최상호 (인)

부위원장 하남출 (인)

위원 최영진 (인)

ABSTRACT

Glycogen branching enzyme (GBE) is a branching enzyme that catalyzes the formation of α-1,6-branching points during glycogenesis by cleaving α-1,4 bond and making a new α-1,6 bond. Most GBEs belong to glycoside hydrolase 13 family, but new GBEs in the glycoside hydrolase 57 family (GH57) were isolated in archaebacteria. Here, I determine the crystal structure of a GH57 GBE from the hyperthermophilic archaebacteria, *Pyrococcus horikoshii* (*Ph*GBE). The crystal of *Ph*GBE belongs to $P2_1$ space group at a resolution of 2.3 Å. *Ph*GBE has a central $(\beta/\alpha)_7$-barrel domain that contains an embedded helix domain, and an α-helix-rich C-terminal domain. The active-site cleft is located at the interface of the central domain and the C-terminal domain. Site-directed mutation was performed and the variant enzymes were checked. The iodine assay was applied to measure the enzymatic activities containing branching and hydrolase activities. The branching activity was measured by high-performance anion-exchange chromatography (HPAEC). This assay allows determination of the amount of branch points introduced by measuring the difference in the amount of reducing ends before and after debranching of the product by isoamylase. Mutation at Trp22, which is apart from the catalytic nucleophilic residue, abolished the both enzymatic activities, indicating that Trp22 might be responsible for the substrate recognition. I also observed that the deletion of a flexible loop near the catalytic residue changed the branching length of the product with an increased hydrolase activity. Taken together,

these findings propose molecular mechanism for how the GH57 GBEs exhibit the two activities and where the substrates bind on the enzyme. These findings propose molecular mechanism for how the GH57-type GBEs exhibit the two activities and where the substrates bind on the enzyme. These researches may contribute to understanding how glycogen metabolism progresses in marine and extreme microorganisms and how glycogen metabolism plays a role in survival in the environments. In addition, this study will contribute to the use of GH57 GBE in the food industry.

Keywords: **X-ray crystal structure, *Pyrococcus horikoshii*, glycogen, amylose, branching enzyme**
Student Number: **2015-21770**

CONTENTS

LIST OF FIGURES

LIST OF TABLE

I. INTRODUCTION

Pyrococcus horikoshii is a hyperthermophilic archaeon that were isolated from a deep hydrothermal vent in the Okinawa (Ando et al., 1999; Gonzalez et al., 1998). Studies of archaea provide important data for studying how living things evolved from the origin of life (Gribaldo and Brochier-Armanet, 2006). Marine life is an organism that occupies about 80% of the world's species, and ecological research and industrialization research by using it are insufficient (Rothschild and Mancinelli, 2001). *Pyrococcus* spp. are some of the most studied archaea because of their utility for a variety of biotechnological applications (Synowiecki et al., 2006; Theriot et al., 2011). Researching the characteristics of enzymes produced by extreme environmental microorganisms will contribute to the discovery of industrially useful enzymes (Blumer-Schuette et al., 2008).

Glycogen is highly branched polysaccharides consisting of linear chains of glucose molecules that are linked by α-1,4-glycosidic bond with α-1,6-glycosidic bond at branching points (Francois and Parrou, 2001). Glycogen is a major polysaccharide found in all organisms. Many microorganisms accumulate in the cells as energy storage materials (Preiss, 2009). Therefore, the study of enzymes involved in the synthesis and degradation of glycogen is important in understanding the viability of microorganisms. Glycogen with shorter average chain length is prone to be more slowly degraded, which may be beneficial for the bacteria under starvation condition (Wang and Wise, 2011). In thermophilic bacteria, the short

average chain length of glycogens appears to be more important for storing the energy-rich compound longer in a high temperature environment that could accelerate the metabolism rate (Wang and Wise, 2011).

To synthesize glycogen in bacteria, at least three different enzymes are sequentially entailed (Preiss, 2009; Ugalde et al., 2003). ADP-glucose pyrophosphorylase is initially employed for synthesizing ADP-glucose, and then glycogen synthase synthesizes α-1,4-linear chain of glucose using ADP-glucose. At the last step, glycogen branching enzyme (GBE) introduces the branches in the linear glucose chain (Ugalde et al., 2003). GBE catalyzes the introduction of an α-1,6-glycosidic bond by cleaving α-1,4-glycosidic bond in the linear chain and transferring the non-reducing ends of the cleaved oligosaccharide to the branching point (Boyer and Preiss, 1977; Guan et al., 1997; Seibold et al., 2011). Most GBEs both in eukaryotes and bacteria belong to glycoside hydrolase family 13 family (GH13) (MacGregor et al., 2001; MacGregor and Svensson, 1989; Palomo et al., 2011). However, a new family of GBE was recently identified in the hyperthermophilic archeabacteria *Thermococcus kodakaraensis* KOD1, which was classified as glycoside hydrolase family 57 (GH57) (Henrissat and Bairoch, 1996).

Crystal structure of a GBE from *Mycobacterium tuberculosis* revealed that GH13 GBEs consist of three domains: the N-terminal β-sandwich domain, the central catalytic domain adopting $(\beta/\alpha)_8$-barrel, and the C-terminal β-sandwich domain (Pal et al., 2010). The N-terminal domain affected the average chain length of the product (Binderup et al., 2000; Devillers et al., 2003). However, GH57 GBE

proteins show substantial structural differences from GH13 GBEs (Palomo et al., 2011). The members of GH57 have five conserved regions including two conserved catalytic residues. However, they vary in the number of amino acid residues (Zona et al., 2004). GH57 GBEs are α-retaining enzymes acting via a glycosyl-enzyme intermediate using the double-displacement reaction mechanism (Palomo et al., 2011). The crystal structures of GH57 GBEs from *Thermococcus kodakaraensis* and *Thermus thermophilus* showed many structural features (Palomo et al., 2011; Santos et al., 2011). Unlike GH13 GBE, GH57 GBEs lack the N-terminal domain of GH13 family. Moreover, they have an altered central domain with a rare $(\beta/\alpha)_7$-barrel fold forming the catalytic domain. The C-terminal domain of GH57 GBE consists of five α-helices, which is distinct from the C-terminal domain of GH13 GBE consisting of eight β-sandwich (Santos et al., 2011). GH57 GBEs have both the endo α-1,4-hydrolase activity and the α-1,6-branching activity, and show different average branching lengths of the products. However, it remains to be elucidated the catalytic mechanism for the two enzymatic activities together with how GH57 GBEs has different average branching lengths in the products (Murakami et al., 2006).

A new GH57-type GBE was recently identified from *P. horikoshii* GBE (*Ph*GBE) (Kawarabayasi et al., 1998; Zona et al., 2004). By structural comparison and mutation studies, I suggest a region of substrate binding which is related to the chain length of the glycogen. I also discuss a role of a flexible loop near the active site in the catalytic mechanism of GH57 GBEs. These findings propose molecular

mechanism for how the GH57-type GBEs exhibit the two activities and where the substrates bind on the enzyme. These researches may contribute to understanding how glycogen metabolism progresses in marine / extreme microorganisms and how glycogen metabolism plays a role in survival in the environment.

II. MATERIALS AND METHODS

2.1. Plasmid construction

The DNA coding *Ph*GBE (PH1386, accession number WP_010885475) was amplified by polymerase chain reaction (PCR) from the genomic DNA of *P. horikoshii* using the following two primers (forward: 5'-GGT CAT ATG ATG AAA GGA TAC CTA AC-3'; reverse: 5'- GGT CTC GAG AAG GGT TGA TTT CTT C-3'; the underlined sequences represent the NdeI and XhoI restriction sites, respectively). The amplified product and the expression vector pET-29b (Invitrogen) were digested with NdeI and XhoI restriction enzymes, and the digested product was inserted into the expression vector pET-29b by DNA ligase. The resulting plasmid encodes *Ph*GBE with a C-terminal hexa-histidine tag, and its sequence was confirmed by DNA sequencing.

2.2. Site direct mutagenesis

The loop shortened mutation (deletion of residues 238-247) and single mutation of tryptophan (Trp22) to alanine were performed by the overlapping PCR technique. Each single mutation of glutamate (Glu76) to alanine and glutamate (Glu185) to glutamine were performed using the Quick Change XL Site-directed Mutagenesis

Kit (Ho et al., 1989). After amplification, the PCR mixture was incubated with DpnI at 37℃ for 2 hours. For overexpression of the recombinant DNA, the mutant plasmid was transformed into the *E. coli* XL-1 Blue (DE3) competent cell by heat-shock. The sequence of mutant plasmid was confirmed by automated DNA sequencing. Primers used site direct mutagenesis are presented in Table 1.

2.3. Purification of GBE and variant GBE proteins

2.3.1. Overexpression

To expression of the recombinant proteins, a single colony from the *E.coli* BL21 (GBE WT or E185Q or W22A or E76A or loop shortened mutant) was inoculated into 25 mL LB broth including 50 μg/mL kanamycin (Duchefa, Netherlands) and incubated it at 37℃ for 12 hours. The resultant seed culture was inoculated to 1.5 L of LB medium containing 50 μg/mL kanamycin. The cells were grown at 37℃ until an OD 600 of 0.5 was attained and then induced with 0.5 mM isopropyl 1-thio-β-D-galactopyranoside (IPTG) for 6 h at 30℃. Cells were harvested by centrifugation at 1,380*g* for 10 min, and disrupted by sonication in lysis buffer containing 20 mM Tris-HCl (pH 8.0), 150 mM sodium chloride, and 2 mM β-mercaptoethanol. After disrupting the cells by sonication, the crude lysate was centrifuged at 10,000*g* for 30 min and cell debris was discarded.

2.3.2. Affinity chromatography

The purification was conducted in three steps. The supernatant was applied to Ni^{2+}–NTA affinity resin that had been pre-incubated with lysis buffer. This mixture was then stirred for 1 h at 4°C. After the mixture was stirred on the column, the non-bound fraction was washed off with lysis buffer supplemented with 20 mM imidazole. The target protein was eluted with 25 mL of lysis buffer supplemented with 250 mM imidazole. The eluted fractions containing GBE were collected.

2.3.3. Ion-exchange chromatography

The eluted recombinant proteins were diluted by the lysis buffer at 1:4 ratio. The diluted protein sample was loaded to ion exchange chromatography on Hitrap Q column (GE Healthcare, USA). The protein was eluted from the column with a linear gradient of 0–1 M NaCl in lysis buffer.

2.3.4. Size exclusion chromatography

As a final purification step, gel filtration was performed using HiLoad Superdex 200 columns (GE Healthcare, USA) pre-equilibrated with 20 mM Tris-HCl pH 8.0 buffer containing 150 mM NaCl and 2 mM 2-mercaptoethanol. The purified proteins were concentrated until 7 mg/ml using Vivaspin 20 (Sartorius, Germany).

2.4. Crystallization

Initial crystallization screen of GBE was performed by the sitting-drop vapor-diffusion method using commercial screening solution from Documents Hampton Research and Anatrace. The sitting drops were mixed with 200 nL drops consisting of a 1:1 ratio of protein by using mosquito robot (TTP Labtech, United Kingdom) and equilibrated against 60 μl reservoir solution at 14°C. The crystals of GBE were obtained in the precipitant solution containing 20 mM citric acid, 80 mM Bis-Tris propane pH 8.8, 16% (w/v) PEG 3350, 2 mM tris (2-carboxyethyl) phosphine (TCEP). To improve the quality of the crystals, two components of initial condition were optimized by varying the precipitant concentration and pH using hanging-drop vapor-diffusion method. Large single crystals of GBE were obtained in 3 days from a solution containing 20 mM citric acid, 80 mM Bis-Tris propane pH 9.3, 10% (w/v) PEG 3350, and 2 mM TCEP by mixing equal volumes (1 μl) of protein and reservoir solutions equilibrated against 500 μl of reservoir solution.

2.5. Structure determination and refinement

The crystals of *Ph*GBE were cryoprotected by precipitation solution adding 20% (v/v) glycerol and then frozen in liquid nitrogen at -173°C (Jo et al., 2015b). The X-ray diffraction data were collected on the beamline 5C of the Pohang Accelerator

Laboratory. Diffraction data were indexed, integrated, and scaled using the HKL2000 software (Otwinowski and Minor, 1997). The crystal belongs to $P2_1$, with unit-cell dimensions of a = 120.9 Å, b = 42.3 Å, c = 122.2 Å. The structure was solved by the molecular replacement method using the coordinates of branching enzyme from *Thermococcus kodakaraensis* (PDB code: 3N8T) as a search model with MOLREP within CCP4 package (Evans, 2011). The model was built with the program COOT and refined with PHENIX refinement (Adams et al., 2002; Emsley and Cowtan, 2004). The final model was refined at 2.3 Å, resulting in an R factor = 19.9%, R_{free} = 25.9%. Further details on the structural determination and refinement are given in Table 2.

2.6. Iodine assay

The iodine assay was applied to measure the total enzymatic activities containing branching or transglycosylation and hydrolytic activities (Guan and Preiss, 1993). The assay is based on monitoring the decrease in absorbance of the glucan-iodine complex resulting from the branching of amylose. The total activities of the enzyme were measured using amylose from potato (Sigma, USA) as a substrate. The amylose powder was dissolved 20 mg in 200 µl ethanol and added 2 ml water and 400 µl of 10% NaOH. Then the amylose sample was heated in boiling water bath until sample dissolves and cooled to ambient temperature. The final sample was diluted to 20mL with water and final concentration was 1 mg/ml in 1% ethanol and

50mM NaOH. I used 0.05 mg/ml amylose in 25 mM sodium acetate buffer at pH 6.5 as the substrate with 160 nM PhGBE and E185Q variant enzyme (Jo et al., 2015a). The reaction temperature was 70 ℃. The reaction mixture (100 μl) was mixed with iodine solution (lugol solution; Sigma, USA) (200 μl) per 5 minutes. The activity of *Ph*GBE native enzyme was estimated as the decrease in absorbance of at 660 nm.

2.7. Branching assay

The chain length distribution of glucan was analyzed by high-performance anion-exchange chromatography (HPAEC). This method allows determination of the amount of branch points introduced by measuring the difference in the amount of reducing ends before and after debranching of the product by isoamylase (Palomo et al., 2011). It was performed by using 0.2% amylose from potato (Sigma, USA) as a substrate. The substrate was incubated with 50 mM sodium acetate buffer at pH 6 for 20 hours. The reaction temperature was 60 ℃. After the reaction, ethanol was added for 1 hours. Isoamylase was treated the reaction mixture after the ethanol was discarded by rotary vacuum concentration. One unit of GBE branching activity was defined as amount of enzyme that changes the OD value by 0.01 for 1 minute.

Table 1. Primer sequences used for construction of *Ph*GBEs.

Wild type	
Forward	5'-GGTCATATGAAAGGATACCTAAC-3'
Reverse	5'-GGTCTCGAGAAGGGTTGATTTCTTC-3'
E185Q	
Forward	5'-CATCTGGCTACCTCAGTGTGCCTACAG-3'
Reverse	5'-CTGTAGGCACACTGAGGTAGCCAGATG-3'
W22A	
Forward	5'-CATGGAAAAGCGCTTTTGGAGAG-3'
Reverse	5'-CTCTCCAAAAGGCGCTTTTCCATG-3'
E76A	
Forward	5'-GAATATATAAAGAGGGCCTTCGAGAAGTAC-3'
Reverse	5'-GTACTTCTCGAAGGCCCTCTTTATATATTC-3'
Loop shortened mutant	
Forward	5'-AGCTTAAGGTATGGAACTCTCAGACCTTAC-3'
Reverse	5'-GTAAGGTCTGAGAGTTCCATACCTTAAGCT-3'

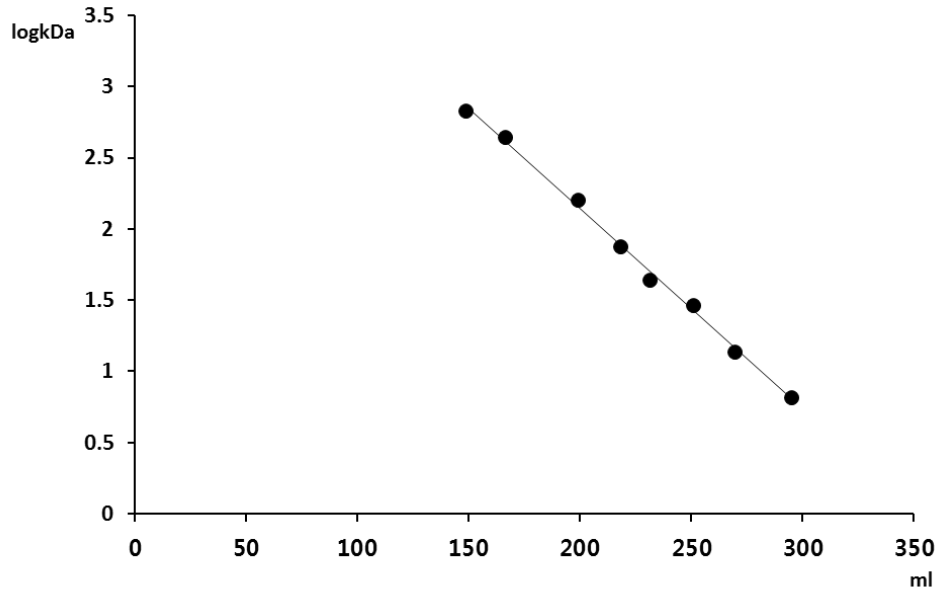

Figure 1. A standard curve of size exclusion chromatography. 148.5 ml : thyroglobulin (669 kDa), 166.21 ml : ferritin (440 kDa), 199.1 ml : Aldolase (158 kDa), 218.23 ml : Conalbumin (75 kDa), 231.27 ml : Ovalbumin (44 kDa), 250.82 ml : carbonic anhydrase (29 kDa), 269.66 ml : Ribonuclease A (13.7 kDa), 294.97 ml : aprotinin (6.5kDa)

III. RESULTS

3.1. Overexpression and purification of GBE and variant GBE proteins

*Ph*GBE (560 amino acid residues) and the variant GBEs were expressed in *E. coli* BL21 (DE3) and purified using subsequent chromatographic steps to homogeneity. The proteins contain the hexa-histidine tag at the C-terminus of the protein. The variant GBEs were concentrated until 5 mg/ml. Then the native *Ph*GBE sample was purified by gel-filtration using HiLoad 16/60 Superdex 200 column for structural study. The purified protein behaved as a monomer in solution, estimated by the size-exclusion chromatography (Fig. 2). Each steps of purifications were monitored by SDS–PAGE (Fig. 3, 4).

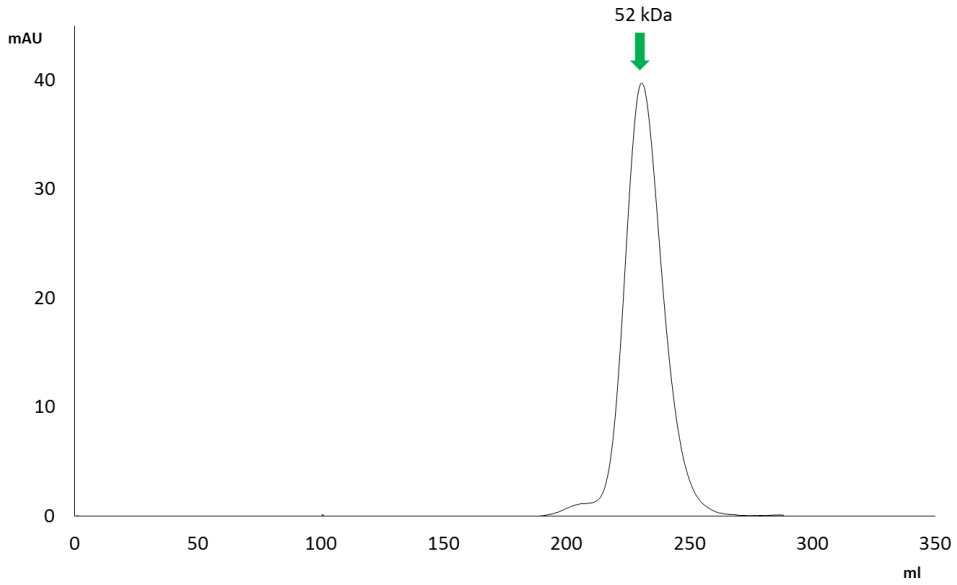

Figure 2. Elution profile of *Ph*GBE on a size exclusion chromatography.

Size exclusion chromatography was performed using HiLoad Superdex 200 columns (GE Healthcare, USA). The peak indicates 52 kDa, which corresponds to the monomeric size. The molecular weight was calculated using a standard curve (Fig. 1).

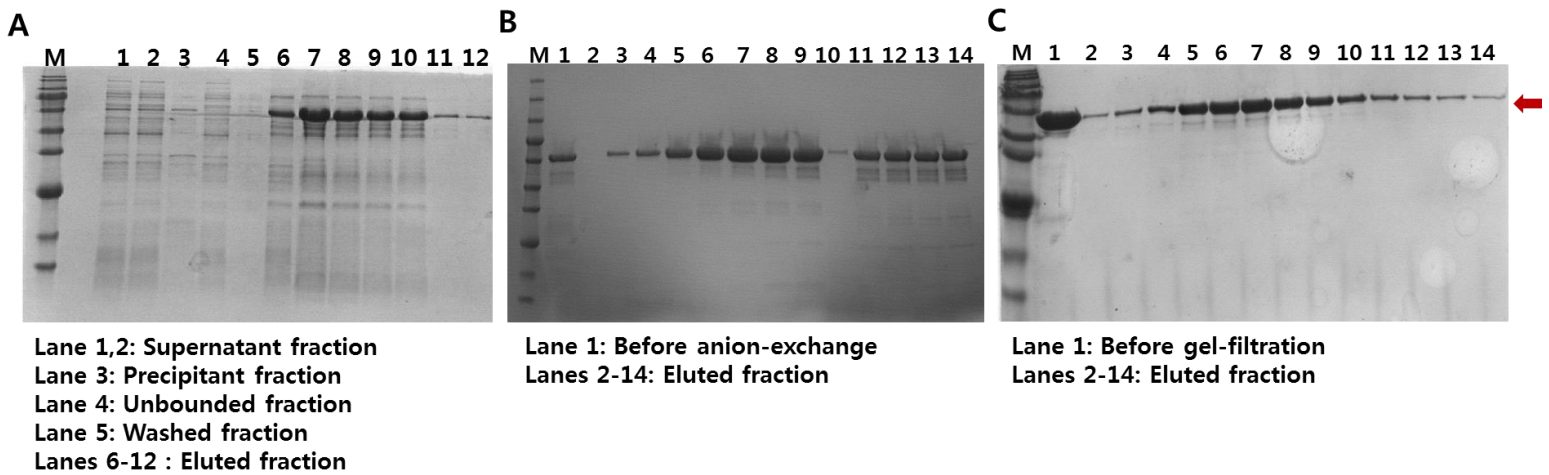

Figure 3. Purification profile of *Ph*GBE from the Ni-NTA chromatography (A), the anion-exchange chromatography (B), and the size-exclusion chromatography (C). The arrow indicates PhGBE size.

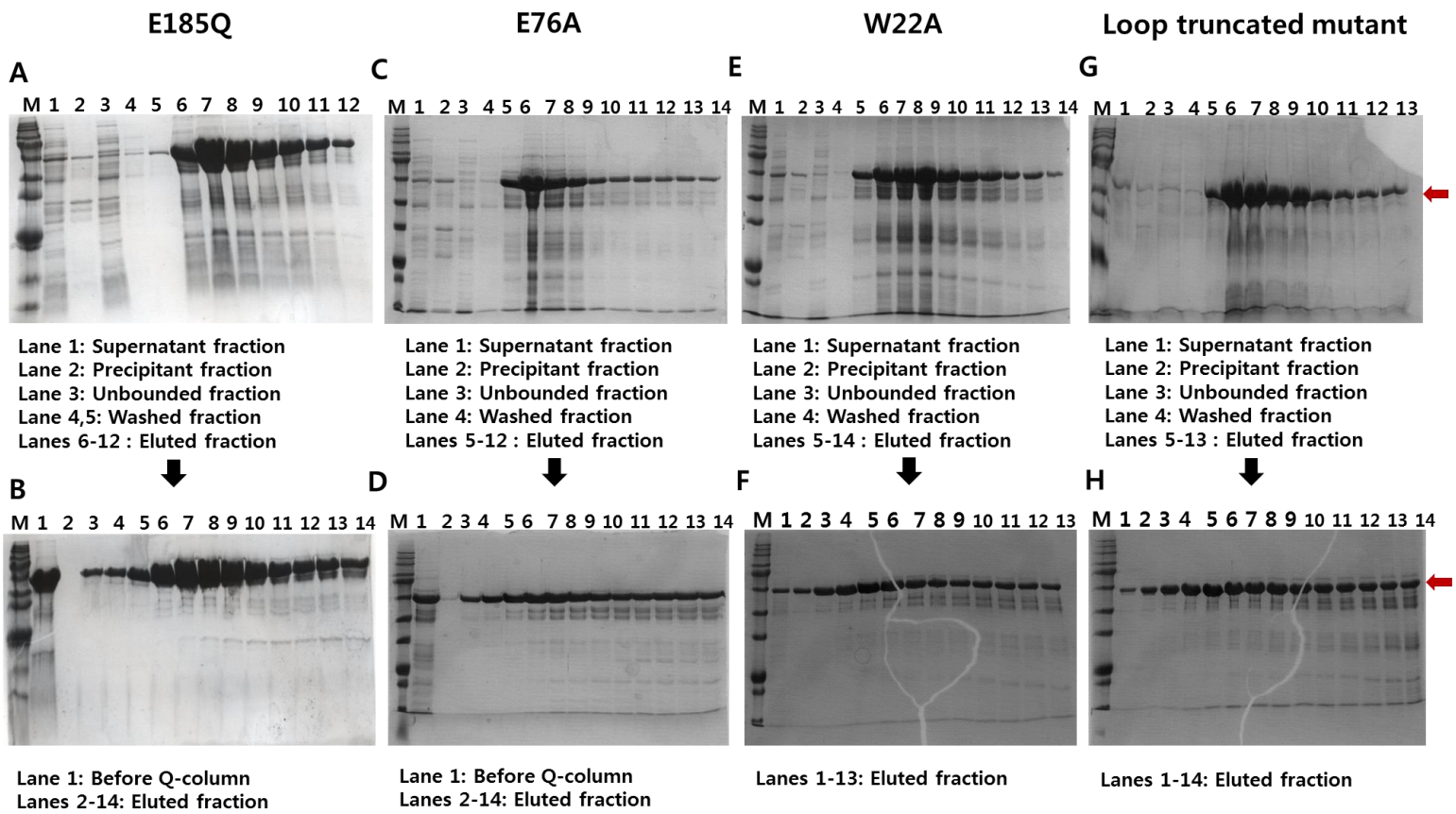
E185Q
E76A
W22A
Loop truncated mutant
A
M 1 2 3 4 5 6 7 8 9 10 11 12
Lane 1: Supernatant fraction
Lane 2: Precipitant fraction
Lane 3: Unbounded fraction
Lane 4,5: Washed fraction
Lanes 6-12 : Eluted fraction
B
M 1 2 3 4 5 6 7 8 9 10 11 12 13 14
Lane 1: Before Q-column
Lanes 2-14: Eluted fraction
C
M 1 2 3 4 5 6 7 8 9 10 11 12 13 14
Lane 1: Supernatant fraction
Lane 2: Precipitant fraction
Lane 3: Unbounded fraction
Lane 4: Washed fraction
Lanes 5-12 : Eluted fraction
D
M 1 2 3 4 5 6 7 8 9 10 11 12 13 14
Lane 1: Before Q-column
Lanes 2-14: Eluted fraction
E
M 1 2 3 4 5 6 7 8 9 10 11 12 13 14
Lane 1: Supernatant fraction
Lane 2: Precipitant fraction
Lane 3: Unbounded fraction
Lane 4: Washed fraction
Lanes 5-14 : Eluted fraction
F
M 1 2 3 4 5 6 7 8 9 10 11 12 13
Lanes 1-13: Eluted fraction
G
M 1 2 3 4 5 6 7 8 9 10 11 12 13
Lane 1: Supernatant fraction
Lane 2: Precipitant fraction
Lane 3: Unbounded fraction
Lane 4: Washed fraction
Lanes 5-13 : Eluted fraction
H
M 1 2 3 4 5 6 7 8 9 10 11 12 13 14
Lanes 1-14: Eluted fraction

Figure 4. Purification profile of variant *Ph*GBEs from the Ni-NTA chromatography (E185Q; A, E76A; C, W22A; E, Loop shortened mutant; G), the anion-exchange chromatography (E185Q; B, E76A; D, W22A; F, Loop shortened mutant; H). The arrow indicates PhGBE size.

3.2. Crystallization of GBE

The final purified sample of the *Ph*GBE protein were concentrated up to 7 mg/ml for the crystallization. The crystals of the full-length *Ph*GBE protein were obtained in the precipitant solution containing 20 mM citric acid, 80 mM Bis-Tris propane pH 9.3, 10% (w/v) PEG 3350, and 2 mM TCEP. To improve the quality of the crystals, I added 10 mM glucose in the optimized crystal conditions of GBE (Fig. 5). After 2 weeks, the GBE crystals were flash-frozen using the cryoprotectant by precipitation solution adding 20% (v/v) glycerol in a nitrogen stream at −173°C.

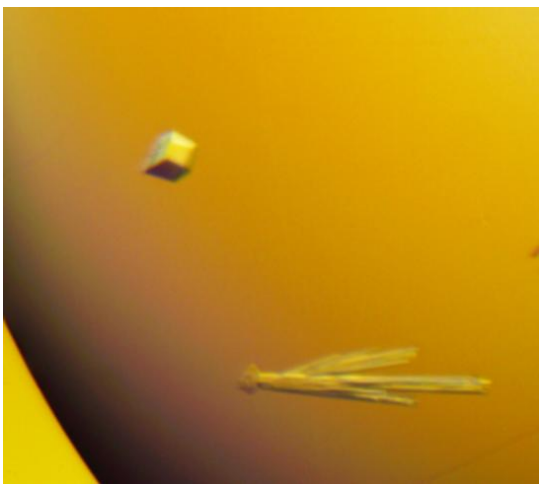

Figure 5. The crystals of *Ph*GBE.

3.3. Structural determination of PhGBE

The crystals of *Ph*GBE belong to $P2_1$ space group, with unit-cell dimensions of a = 120.9 Å , b = 42.3 Å , c = 122.2 Å , and β = 91.0°. The structure was solved by the molecular replacement method using the GBE from *T. kodakaraensis* as a search model (Santos et al., 2011). The final model was refined against the 2.3 Å resolution data set, resulting in an R factor of 0.199 and R_{free} of 0.259. The asymmetric unit in the crystal contain two molecules, and the final model comprises the whole proteins except for residues 231-244 for the corresponding electron density maps were not visible. Further details on the structural determination and refinement are given in Table 2.

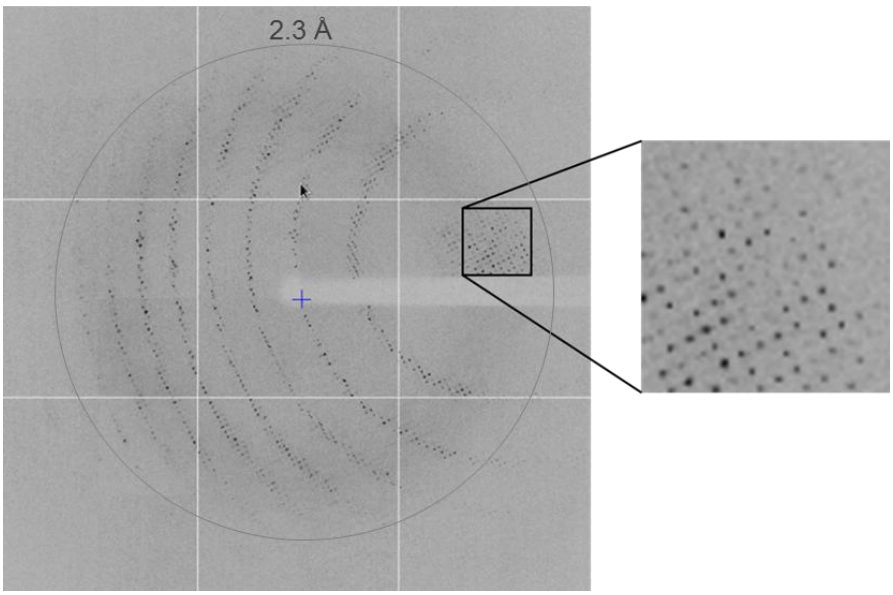

Figure 6. X-ray diffraction image of *Ph*GBE.

Table 2. X-ray statistics for data collection and refinement

	***Ph*GBE**
Data collection	
Space group	$P2_1$
Cell dimensions	
a, *b*, *c* (Å)	120.9, 42.3, 122.2
α, β, γ (°)	90.0, 91.0, 90.0
Resolution (Å)	50-2.30(2.34-2.30)
R_{merge}	0.130(0.383)
$I/\sigma I$	10.2(2.08)
Completeness (%)	95.0(72.1)
Redundancy	5.5(3.7)
Refinement	
Resolution (Å)	33.5-2.3
No. of reflections	44048
R_{work}/R_{free}	0.199/0.259
No. of total atoms	9009
No. of ligands	2
No. of water molecules	96
Wilson B-factor (Å)	29.1
R.M.S deviations	
Bond lengths (Å)	0.003
Bond angles (°)	0.55
Ramachandran plot	
Favored (%)	95.5
Allowed (%)	4.5
Outliers (%)	0.1
Molecules in asymmetric unit	2

* Values in parentheses are for the highest-resolution shell.

R_{free} value was calculated using a test set size of 9.95%.

3.4. Overall structure of PhGBE

The overall structure of the *Ph*GBE shows a triangular shape, like other GH57-type branching enzyme (Fig. 7) (Palomo et al., 2011; Santos et al., 2011). *Ph*GBE consists of three domains; the central $(\beta/\alpha)_7$-barrel domain, two-helix domain, and C-terminal domain. The central $(\beta/\alpha)_7$-barrel domain is a modified version of the $(\beta/\alpha)_8$-barrel structure (or TIM-barrel structure) that is a common feature of other amylases. The $(\beta/\alpha)_7$-barrel domain is also found in glycoside hydrolase 117 (Watanabe et al., 2006). The central domain contains an extra and longer α-helix (α10) next to the $(\beta/\alpha)_7$-barrel structure, which forms an edge of the triangular shape of the protein. The $(\beta/\alpha)_7$-barrel structure was partly distorted by the addition of β-hairpin (β4 - β5) between β3 strand and α7 helix, which was proposed to interrupt oligomerization of GH57 GBE (Santos et al., 2011).

The second domain, called two helix domain, is composed of two α-helices (α3 and α4), and is inserted between α2 and α5 of the central $(\beta/\alpha)_7$-barrel domain. This domain is protruded from the central from the $(\beta/\alpha)_7$-barrel domain, forming another edge of the triangular shape. The central domain and the two helix domain form a catalytic pocket between them. The third C-terminal domain consists of five alpha-helices (α13, α14, α15, α16, and α17), which are arranged in the sequential anti-parallel manner. This domain is located above the triangular shape containing the other domains, and makes a close contact with the active site region in the $(\beta/\alpha)_7$-

barrel domain. The C-terminal α-helical domain is not found in other type of α-amylases.

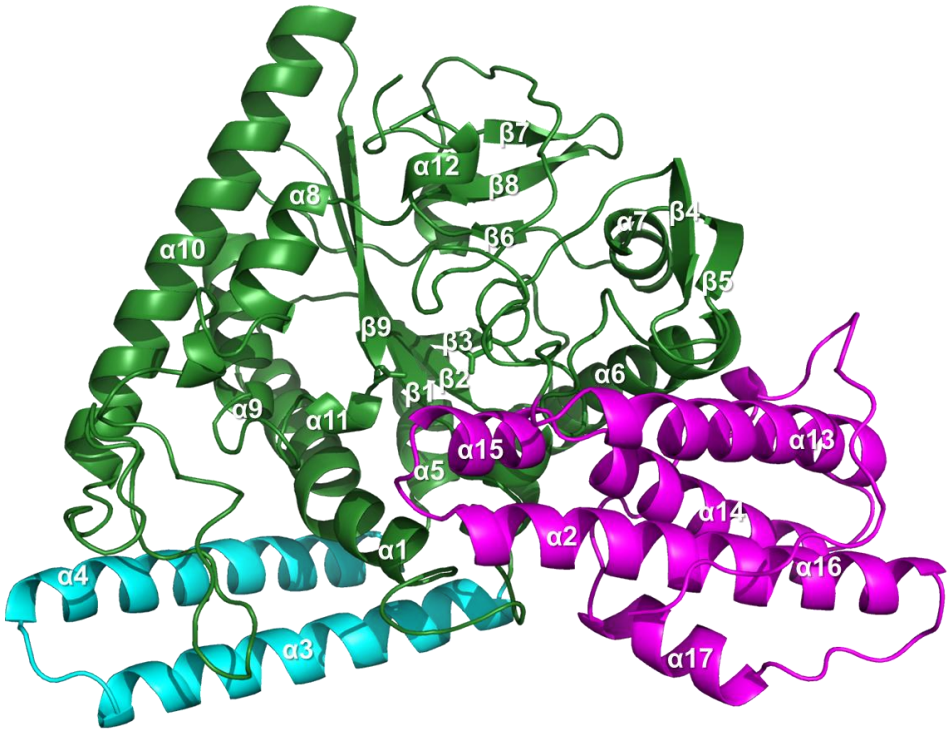

Figure 7. Overall structure *Ph*GBE. The overall structure of *Ph*GBE in the cartoon representation. The central $(\beta/\alpha)_7$-barrel domain (residues 1-70, 123-420) is colored in green, inserted two-helix domain (residues 71-122) is in cyan, and the C-terminal domain (residues 421-550) is in magenta. Each secondary structural element is labeled.

3.5. Structural Comparison with other GH57 proteins

All GH57 proteins exhibit α-amylase specificity at present despite the variation in the sequence among them (Janecek and Kuchtova, 2012). The structure of *Ph*GBE was superposed onto GH57 proteins whose structures are available: AmyC from *Thermotoga maritima*, *Tk*GBE, and *Tt*GBE (Fig. 8).

AmyC is known to have only hydrolase activity on amylose without the branching activity, but its accurate activity is unknown (36% sequence identity) (Dickmanns et al., 2006). In structural comparison with AmyC, the overall structures are almost triangular shape and the three domains are similar. The differences were largely seen in three place. The flexible loop which is disordered in *Ph*GBE and β-hairpin (β4 - β5) loop of *Ph*GBE is not observed in AmyC (Fig. 8A). However, Tyr236 which is located at flexible loop is conserved. AmyC also has much longer flexible loop (residues 267-286) which is located between α9 and α10 in *Ph*GBE. In *Ph*GBE, the long groove that has the center of the active site until the part where Trp22 exists. However, AmyC has a structure in which the bottom surface is clogged (Fig. 9).

*Ph*GBE displays the highest structural similarity to the *Tk*GBE (66% sequence identity) (Santos et al., 2011). The structures of the three GH57 GBEs were very similar. The superposition of *Ph*GBE to *Tk*GBE structures reveals the high similarity of all three domains (Fig. 8B). *Tk*GBE has shorter inserted domain (α4) and top of the N-terminal domain (α10) than *Ph*GBE and *Tk*GBE. *Tk*GBE has

shorter inserted domain (α4) than *Ph*GBE. The flexible loop is ordered in *Tk*GBE structure which is the complex structure with glucose.

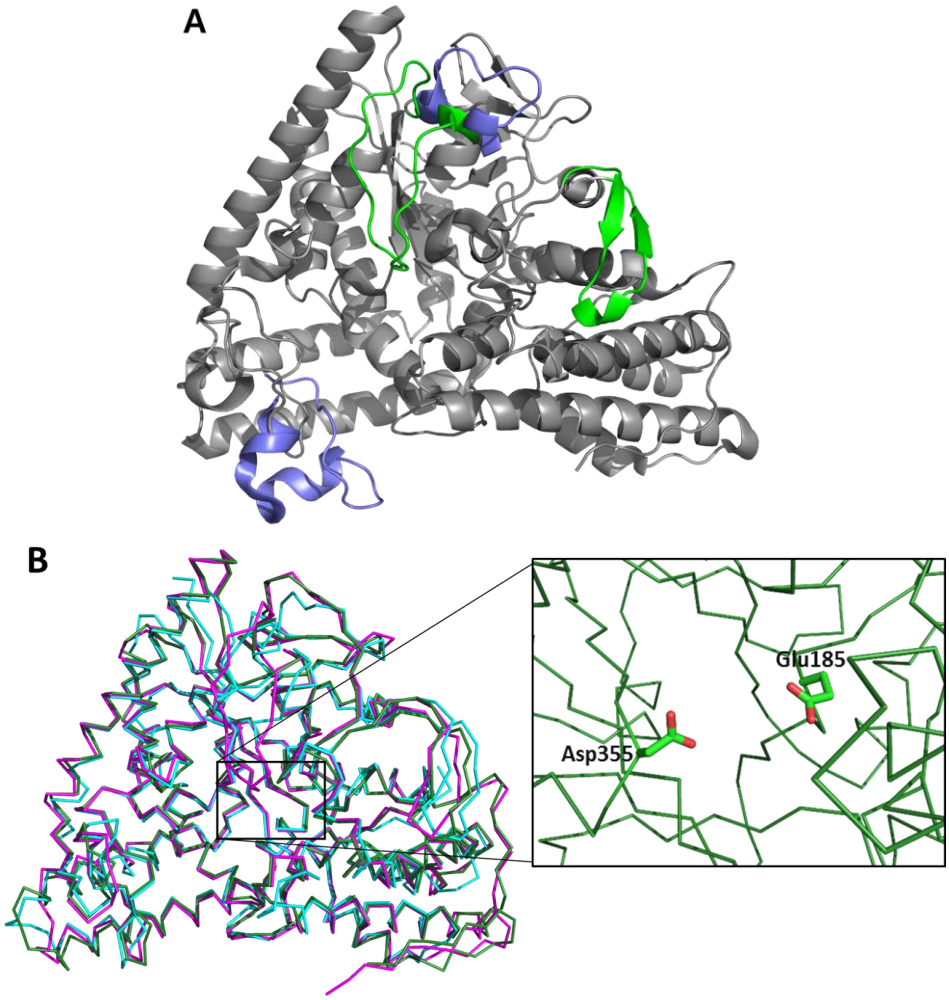

Figure 8. Structural superposition of *Ph*GBE with its homologous proteins. A. *Ph*GBE structure in cartoon representation s superposed on AmyC from *Thermotoga maritima* (PDB code 2b5d), which is GH57-type enzyme. Differences in each comparison are colored in green for *Ph*GBE and blue for AmyC. B. *Ph*GBE structure in ribbon representation (green) is superposed on GBE from *Thermococcus kodakaraensis* (magenta; PDB code 3N98), and GBE from *Thermus*

thermophiles (cyan; PDB code 3p0b). The active site region containing two key catalytic residues (Glu185 and Asp355) in stick representation are indicated by a black rectangle.

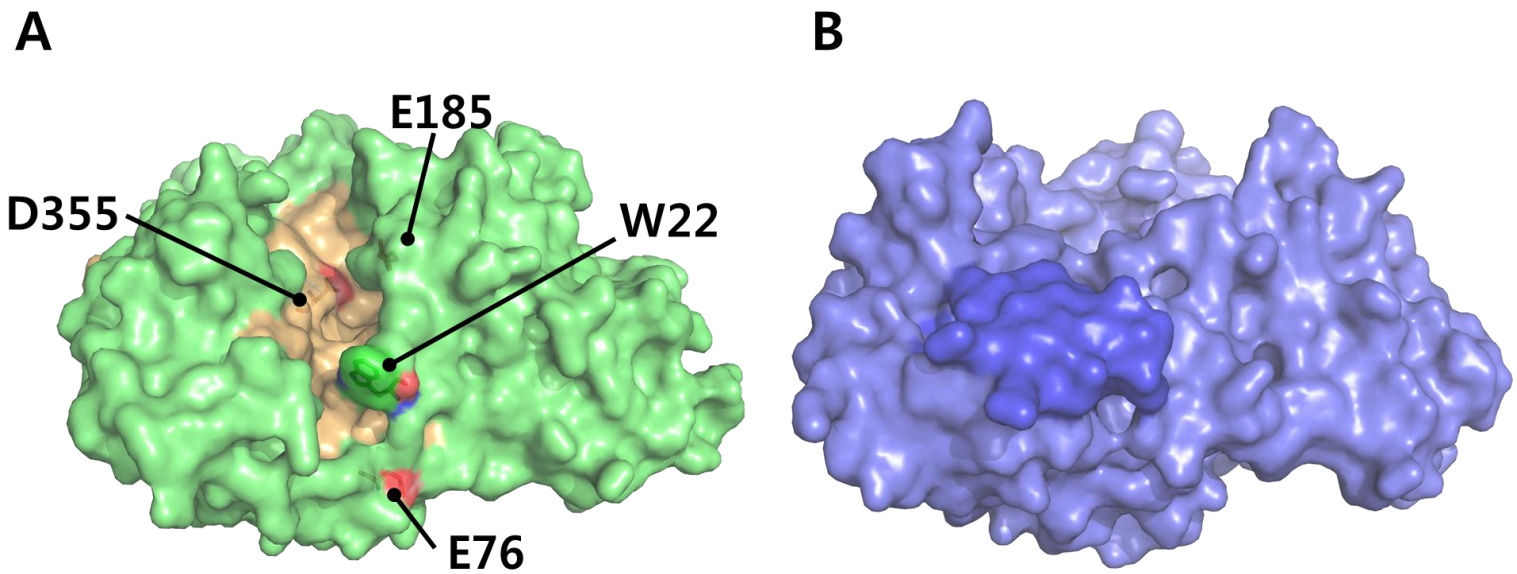

Figure 9. Bottom surface structure of *Ph*GBE (green; A) and AmyC (blue; B). Catalytic residues (E185, D355) and point mutation candidate residues (W22, E76) are shown in the stick representation. The clogged part of AmyC is colored by dark blue.

3.6. The active site of PhGBE

The structural and sequence alignments of *Ph*GBE with other GH57 GBEs from *T. kodakaraensis* and *T. thermophilus* (TkGBE and TtGBE, respectively) unambiguously identified the active site region with the two catalytic residues (Glu185 and Asp355; Fig. 8B) (Zona et al., 2004). As shown in Fig. 10, a long and bent groove is observed in the active site region of *Ph*GBE. The two catalytic residues (Asp355 and Glu185) are shown at the left and right sides of the bending point of the cleft. Catalytic general acid/base residue Asp355 is at the end of the β10 and the nucleophilic residue Glu185 is at the loop between α6 and the inserted β4, β5 hairpin. To confirm the role of catalytic residues, I generated a mutant *Ph*GBE that harbors mutation at Glu185 with glutamine residue. To measure the total activity of GBE, I conducted the iodine assay using amylose as a substrate. When amylose is hydrolyzed or branched, the absorbance at 660 nm is decreased (Guan and Preiss, 1993). The mutant *Ph*GBE abolished the enzymatic activity of *Ph*GBE, which confirmed the catalytic role of Glu185 (Fig. 11).

I found many tryptophan, histidine, and phenylalanine residues (Trp28, Trp272, His288, Trp362, Trp363, Trp408, Trp417, His325, His328, His361, and Phe471) near the catalytic residues of *Ph*GBE (Fig. 10). Active site surface of many carbohydrate modifying enzymes are decorated with tryptophan and histidine residues for attachment of the glucose units of the substrates (Tormo et al., 1996).

Thus these tryptophan and histidine residues in *Ph*GBE are likely to be involved in recognizing the substrate amylose (Santos et al., 2011).

The long groove lined with the catalytic residues is suggested to be substrate binding site (Fig. 10). Trp22 is at the bottom region of the groove far from the catalytic site and also conserved in GH57 *Tk*GBE and *Tt*GBE. I selected another residue Glu76 which is located outsides of the groove. The Glu76 residue is replaced with other amino acids in other GH57-type GBEs. Therefore, two mutants were prepared and the respective proteins were purified. When the Trp22 residue of *Ph*GBE was mutated into alanine residue, no absorbance difference was observed in the iodine assay compared to the substrate amylose, demonstrating the complete loss of the activity of the mutant enzyme (Fig. 12). In contrast, mutation of Glu76 to alanine residue did not change the activities of *Ph*GBE. These findings suggest that Trp22 plays a crucial role in the catalysis of *Ph*GBE presumably by binding the substrates in the grooves, and the outside of the groove may not be involved in the catalysis or the binding to the substrates.

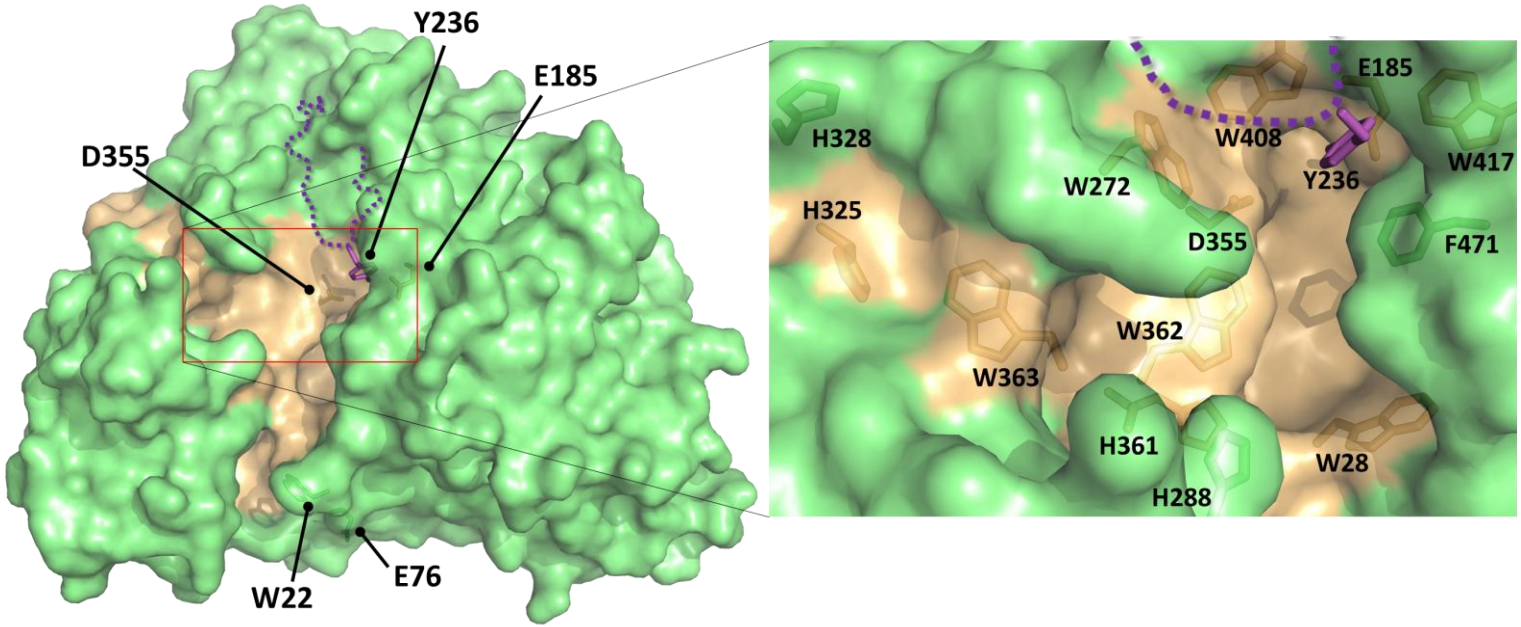
Y236
E185
D355
W22
E76
H328
W408
E185
W417
Y236
W272
H325
D355
F471
W362
W363
H361
W28
H288

Figure 10. Surface structure of *Ph*GBE and active site at the long groove. *Left*, the surface structure of *Ph*GBE (green) and the long groove of *Ph*GBE (yellow). Locations of the two active site residues (Glu185, Asp355) and Trp22 are indicated. The flexible loop (residues 231-244) is disordered in *Ph*GBE, and a possible location was determined by superposition to the structure of *Tk*GBE, which is shown in the magenta broken line. Tyr236 in the flexible loop is in the magenta sticks. The active site region is squared in the red, and is enlarged in the right panel. *Right*, the two catalytic residues (Glu185, Asp355) and the aromatic residues of catalytic pocket (Trp28, Trp272, His288, His325, His328, His361, Trp362, Trp363, Trp408, Trp417, and Phe471) are shown in the stick representation with a transparent surface representation.

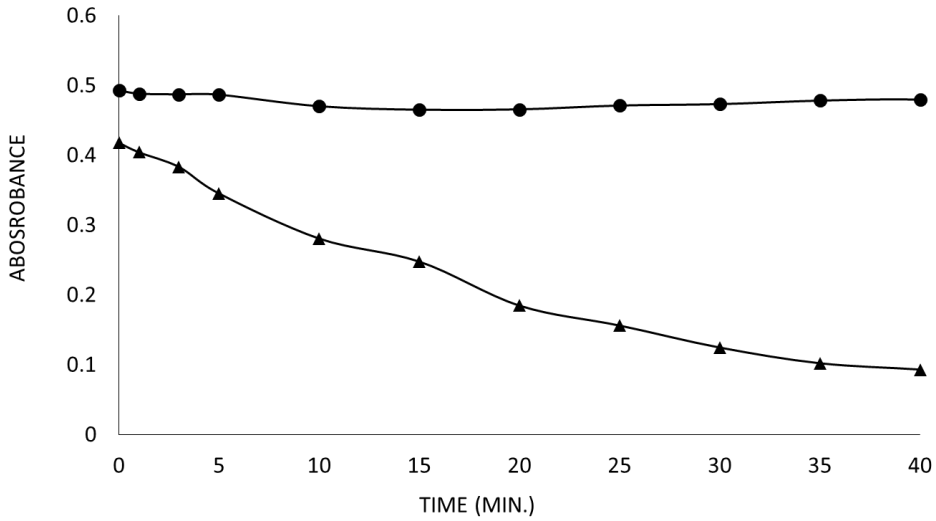

Figure 11. Iodine assay of wild type and E185 variant *Ph*GBEs. Total enzymatic activities of wild type (triangle) and E185Q (circle) were measured by the iodine assay. Amylose was used as a substrate, and would be hydrolyzed or branched by the enzyme. The decrease in the absorbance at 660 nm produced by amylose was calculated as the total activities. 160 nM of the wild type (WT) and E185Q variant of *Ph*GBE were used.

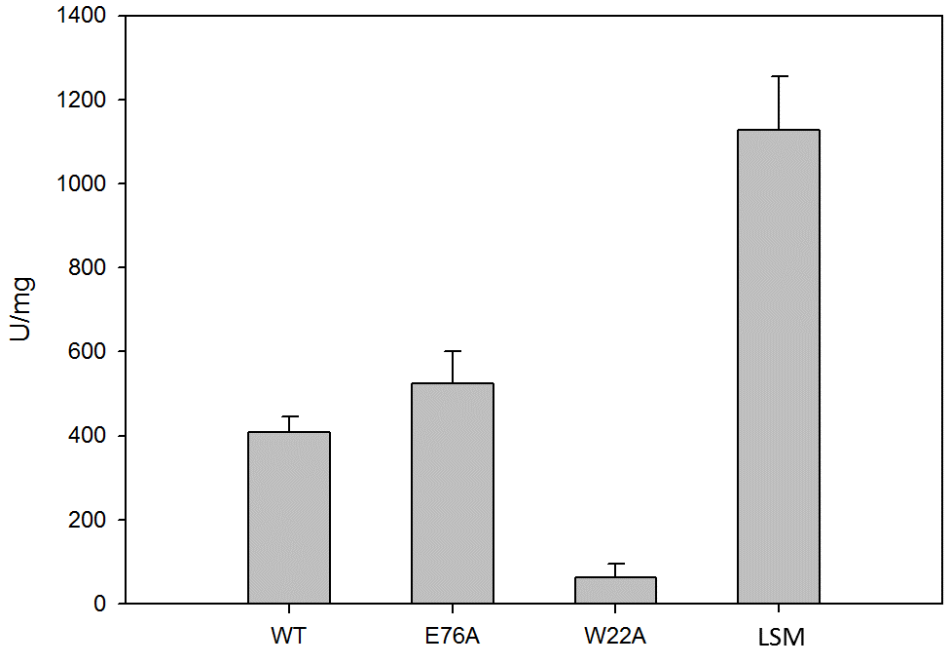

Figure 12. Iodine assay of wild type and variant *Ph*GBEs. To measure the total enzymatic activities, iodine assays were employed. Amylose was used as a substrate, and would be hydrolyzed or branched by the enzyme. LSM indicates loop shortened mutant. The decrease in the absorbance at 660 nm produced by amylose was calculated as the total activities. 3.2 μg of the wild type (WT), E76A, W22A, and 1.7 μg of the loop shortened variants of *Ph*GBE were used. This assay was performed by Minjeong Park from department of microbiology of Pusan National University.

3.7. The role of the flexible loop in the catalysis

A flexible loop (residues 231-244), which is disordered in the crystal structure of *Ph*GBE, is at the top region of the active site groove. In contrast, the loop was displayed in the crystal structure of *Tk*GBE (66% sequence identity). By structural superposition with *Tk*GBE (Palomo et al., 2011), the flexible loop of *Tk*GBE was positioned in the *Ph*GBE structure (Fig. 10) (Santos et al., 2011). The flexible loop of *Ph*GBE contains Tyr236 residue that are invariant among other GH57 GBEs at its tip region is close to the catalytic residues Glu185 and Asp355. Tyr236 was proposed to interact with the cleaved products during the transglycosylation process of the enzyme (Santos et al., 2011). To gain insight into the functional role of the flexible loop, I generated a loop shortened mutant *Ph*GBE protein that lacks the loop (residues 238-247). The variant *Ph*GBE exhibited a 2-fold increase in the activities than the wild type enzyme, as judged by the iodine assay (Fig. 12). The products of the *Ph*GBE variants were analyzed by using high-performance anion-exchange chromatography (HPAEC). Prior to HPAEC, the reaction product was treated with isoamylase to cleave all the branches from the reaction product. From this assay, I could know the branching activity and the chain length pattern of product. The result of HPAEC showed that the variant *Ph*GBE protein has a decreased branching activity since the total area of the branched products are diminished in the loop-shortened variant (Fig. 13). In case of the wild type *Ph*GBE, the degree of polymerization (DP) of the products have the peaks at ranges from 10

to 12. However, the loop-shortened mutant *Ph*GBE has the peaks in the range of DP ~17, which indicates that the chain lengths of the products are longer than that of the wild type enzyme. Collectively, these findings suggest that the flexible loop is associated with the catalytic process of GH57 GBEs, and is important role in the branching activity.

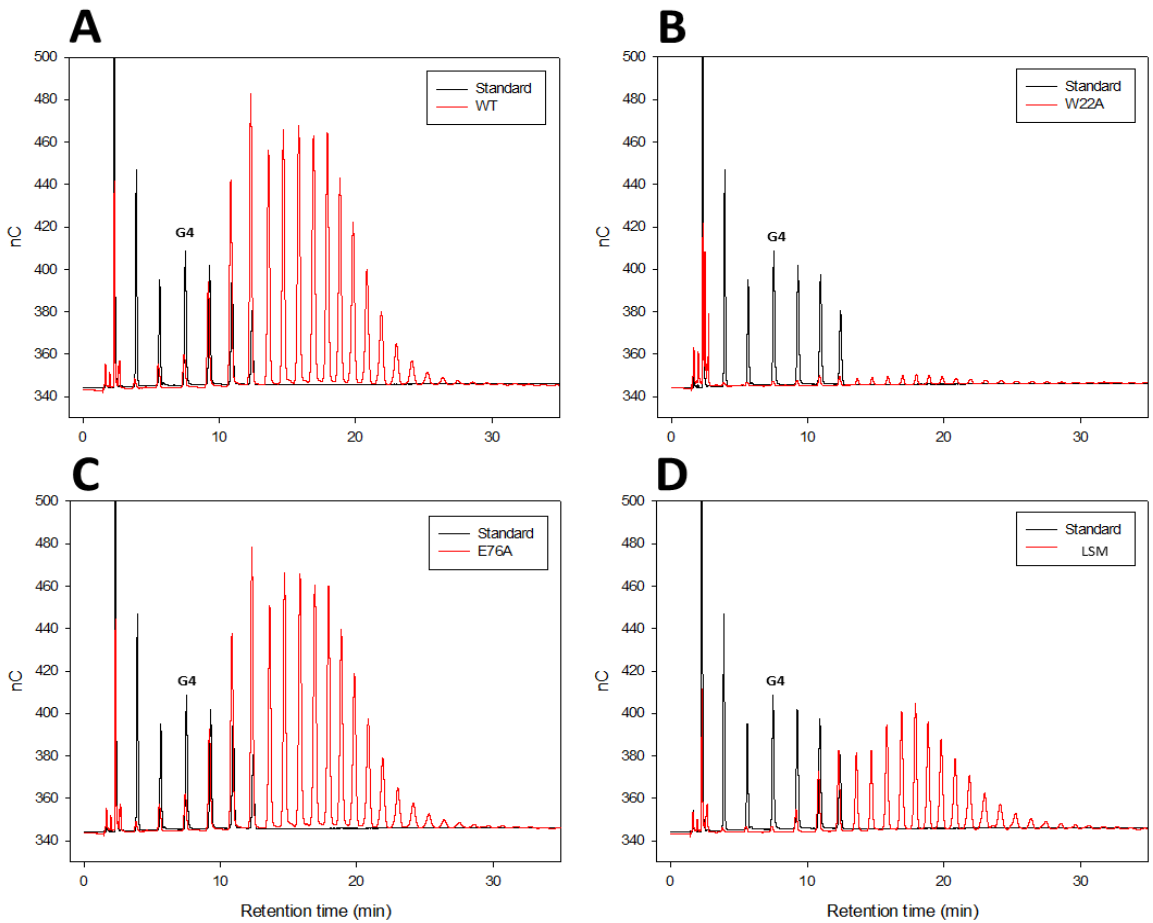
A
B
C
D
Standard
WT
W22A
E76A
LSM
G4
nC
Retention time (min)

Figure 13. Isoamylase assay of wild type and variant *Ph*GBEs. Analysis of the products of *Ph*GBE WT (A), W22A (B), E76A (C) and loop shortened mutant (D) by the HPAEC**.** LSM indicates loop shortened mutant. The analysis of the enzyme reaction products after isoamylase treatment. The black line indicates G1-G7 (glucose - maltoheptaose) standard. Maltotetraose is labeled by G4 above the peak. This assay was performed by Minjeong Park from department of microbiology of Pusan National University.

IV. DISCUSSION

*Ph*GBE has dual activities including the hydrolase and the branching activities. The crystal structure of *Ph*GBE shows triangular shape, and consists of three domains like other homologues GH57 GBEs. A long groove of *Ph*GBE is decorated with aromatic residues on the surface and were expected to be responsible for the substrate binding. The groove is bent near the catalytic residues whose crucial role was confirmed biochemically. Trp22 residue was found at one end region of the groove.

Very interestingly, Trp22 played the essential roles in the catalysis, suggesting that Trp22 may be directly involved in binding of the substrate at the end of the groove. A flexible loop that contains an invariant tyrosine residue (Tyr236) is close proximity to the catalytic residues. Tyr236 was previously characterized to be involved in the branching activity in *Tt*GBE (Palomo et al., 2011). Consistently, this study observed that deletion of the flexible loop increased the total activities of the enzyme, while the deletion mutant exhibited a decreased branching activity (Fig. 12 and 13). The length of flexible loop and the location of Tyr236 may be crucial factor of altering the branching activity.

To explore the action mechanism of *Ph*GBE, I modeled a long linear chain of glucose that are linked by α-1,4-glycosidic bonds on the groove (Fig. 14). In the modeled structure, the non-reducing end of the substrate are interacted by the Trp22

residue at one end of the groove. The six glucose units were fitted to the half of the groove that are from Trp22 to the bending point of the groove. The bending point has the two catalytic residues and Tyr236 from the flexible loop, and thus this region is suggested to be the place where all the catalytic processes occur. In *Tt*GBE, a maltotriose unit was modeled at the bending points (Palomo et al., 2011), which is analogous to the modeling in this study. Another six glucose unit can be modeled on the last half region of the groove that are lined with aromatic residues. The Fig. 14B depicts the intermediate step of the branching process of the enzyme. The nucleophilic residue Asp355 attacks on the C1 atom of the glucose unit making a covalent intermediate between the enzyme and substrate. In the branching process, the cleaved product remains on the groove mainly due to the interaction with Tyr236 in the flexible loop. Alternatively, in case of the hydrolase process, the cleaved product would be released (Fig. 14C). At the last step of the branching process, the OH group attached to C6 atom of the glucose resolves the enzyme-substrate covalent intermediate, resulting in the α-1,6-glycosidic bond (Fig. 14B). In case of hydrolase process, a new water molecule resolves the enzyme-substrate covalent intermediate (Fig. 14C).

Degree of branching and the average length of the branches in glycogen determine its chemical physical properties. Thus the activities of GBE are important in the glycogen synthesis process. In this study, I determined the crystal structure of a newly identified GH57 GBE from *P. horikoshii*, which has both hydrolase and branching activities. The structure showed a high structural similarity to *Tk*GBE,

and displayed the surface groove containing the catalytic residues, the flexible loop, and the Trp22. Based on the structural and biochemical studies, I propose an action mechanism covering the both activities of GH57 GBE. These results would help understand the mechanism of the branching activity and further help design regulate degree of branching and the average length of branches of the product.

Until now, GH13 GBEs have been used extensively in the food industry, such as producing cyclic cluster dextrin (CCD) or changing the solubility of starch (Murakami et al., 2006; Takata et al., 1996a; Takata et al., 1996b). CCD is currently used in the food industry to make sports drinks (Choi et al., 2009). GBE reacts with amylopectin to produce a CCD substance with more branches by cyclization. Since it is possible to bind organic acids to cavities in a helix of CCD, it has the advantage of forming a complex with various functional materials to make a functional beverage. The size of helix of CCD would be varied by changing the branching pattern of GBE. CCD with different size of helix could be combined with other materials of different sizes. This research suggests that by varying the chain length of the GBE product's branch, it can be used to increase the functionality of CCDs industrially, where this study will contribute to the use of GH57 GBE in the food industry.

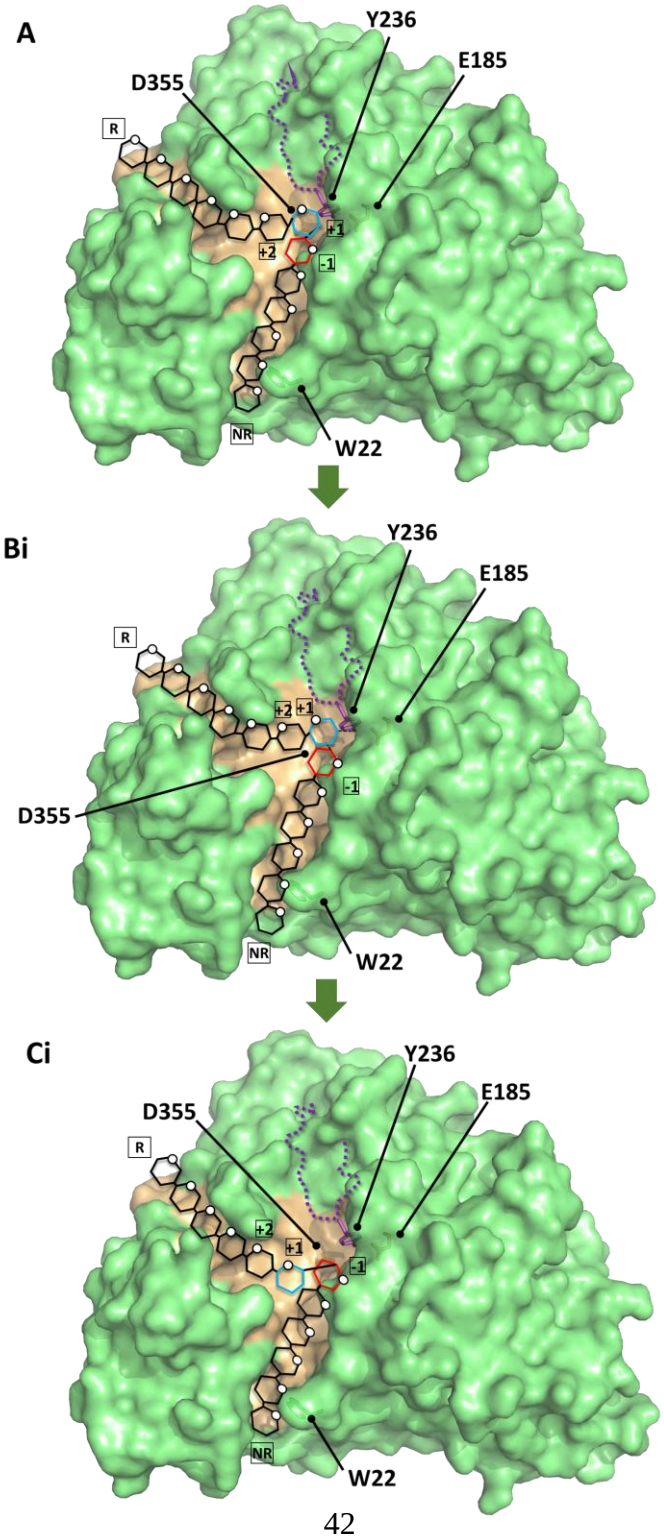
A
Y236
E185
D355
R
+1
+2
-1
NR
W22
Bi
Y236
E185
R
+2
+1
-1
D355
NR
W22
Ci
Y236
E185
D355
R
+2
+1
-1
NR
W22

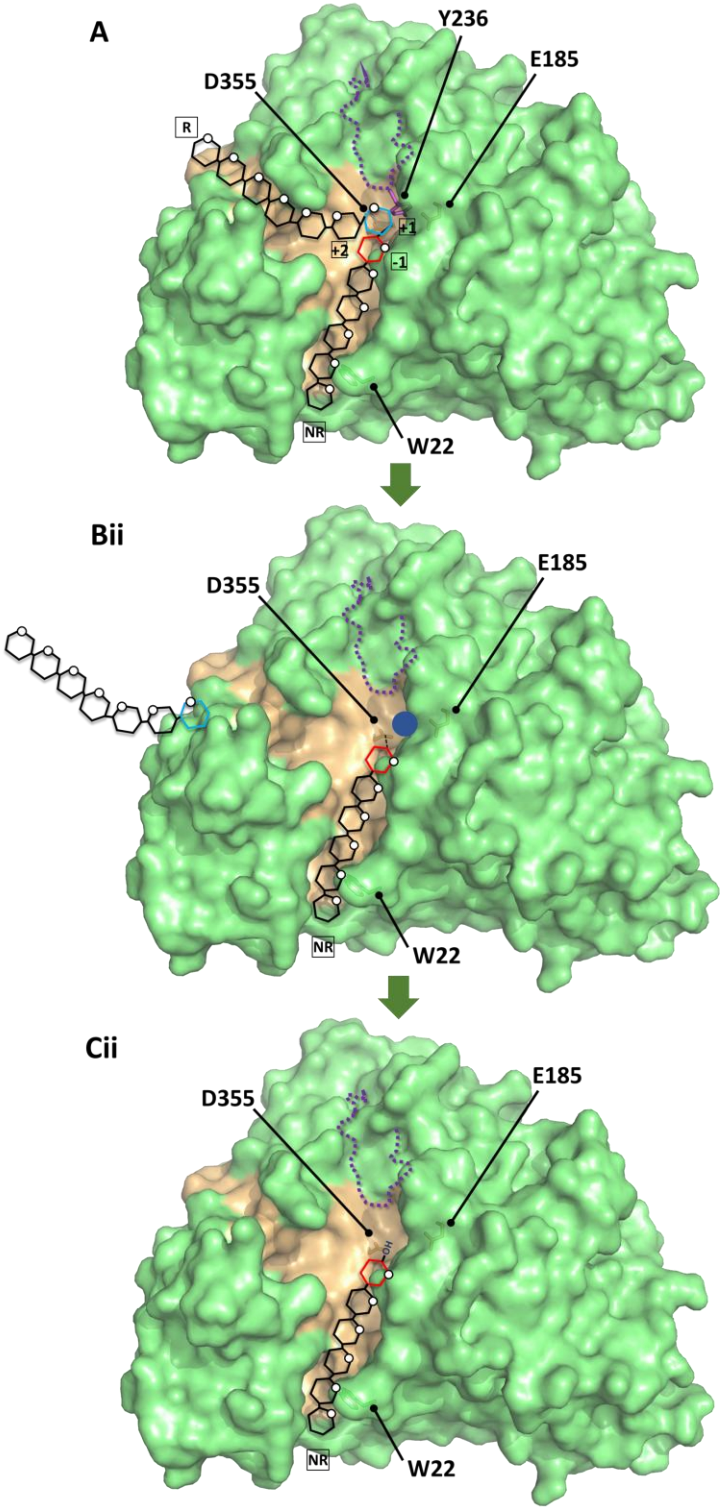
A
Y236
E185
D355
R
+1
+2
-1
NR
W22
Bii
E185
D355
NR
W22
Cii
E185
D355
NR
W22

Figure 14. Proposed mechanisms for the branching and hydrolase activities of GH57 GBEs.

A. The substrate oligosaccharide is bound on *Ph*GBE, which is drawn in the surface representation. Trp22 of *Ph*GBE plays an important role in binding of the oligosaccharide. The long groove is colored in yellow. The reducing end (R) and the non-reducing end (NR), -1, +1, and +2 sites of the oligosaccharide are labeled in squares. Each glucose is represented by regular hexagon with white circle representing oxygen atom. The flexible loop of *Tk*GBE and Tyr236 are shown in magenta. The catalytic residues (Asp355 and Glu185) and Trp22 are labeled.

B. Enzyme-substrate covalent intermediate of the branching process (Bi) and the hydrolysis process (Bii). Asp355 attack on the C1 atom of the glucose at the -1 site, resulting in the covalent intermediates. In the branching process, the cleaved product is still bound via the interaction with Tyr236 in the flexible loop (Bi). In the hydrolysis process, the cleaved product is released from the enzyme (Bii). A water molecule is represented by blue circle.

C. Resolution of the enzyme-substrate covalent intermediate. In the branching process, the OH group attached to the C6 atom of glucose unit at +1 site hydrolyzes the enzyme-substrate covalent intermediate, resulting in formation of the branched product (Ci). In the hydrolysis process, a water molecule (blue) hydrolyzed the intermediate (Cii).

V. REFERENCES

Adams, P.D., Grosse-Kunstleve, R.W., Hung, L.W., Ioerger, T.R., McCoy, A.J., Moriarty, N.W., Read, R.J., Sacchettini, J.C., Sauter, N.K., and Terwilliger, T.C. (2002). PHENIX: building new software for automated crystallographic structure determination. *Acta Crystallogr D Biol Crystallogr 58*, 1948-1954.

Ando, S., Ishikawa, K., Ishida, H., Kawarabayasi, Y., Kikuchi, H., and Kosugi, Y. (1999). Thermostable aminopeptidase from *Pyrococcus horikoshii*. *Febs Lett 447*, 25-28.

Binderup, K., Mikkelsen, R., and Preiss, J. (2000). Limited proteolysis of branching enzyme from *Escherichia coli*. *Arch Biochem Biophys 377*, 366-371.

Blumer-Schuette, S.E., Kataeva, I., Westpheling, J., Adams, M.W., and Kelly, R.M. (2008). Extremely thermophilic microorganisms for biomass conversion: status and prospects. *Curr Opin Biotechnol 19*, 210-217.

Boyer, C., and Preiss, J. (1977). Biosynthesis of bacterial glycogen. Purification and properties of the *Escherichia coli* b alpha-1,4,-glucan: alpha-1,4-glucan 6-glycosyltansferase. *Biochemistry 16*, 3693-3699.

Choi, S.S., Danielewska-Nikiel, B., Ohdan, K., Kojima, I., Takata, H., and Kuriki, T. (2009). Safety evaluation of highly-branched cyclic dextrin

and a 1,4-alpha-glucan branching enzyme from *Bacillus stearothermophilus*. Regul Toxicol Pharmacol *55*, 281-290.

Devillers, C.H., Piper, M.E., Ballicora, M.A., and Preiss, J. (2003). Characterization of the branching patterns of glycogen branching enzyme truncated on the N-terminus. *Arch Biochem Biophys 418*, 34-38.

Dickmanns, A., Ballschmiter, M., Liebl, W., and Ficner, R. (2006). Structure of the novel alpha-amylase AmyC from *Thermotoga maritima*. *Acta Crystallogr D Biol Crystallogr 62*, 262-270.

Emsley, P., and Cowtan, K. (2004). Coot: model-building tools for molecular graphics. *Acta Crystallogr D Biol Crystallogr 60*, 2126-2132.

Evans, P.R. (2011). An introduction to data reduction: space-group determination, scaling and intensity statistics. *Acta Crystallogr D Biol Crystallogr 67*, 282-292.

Francois, J., and Parrou, J.L. (2001). Reserve carbohydrates metabolism in the yeast *Saccharomyces cerevisiae*. *FEMS Microbiol Rev 25*, 125-145.

Gonzalez, J.M., Masuchi, Y., Robb, F.T., Ammerman, J.W., Maeder, D.L., Yanagibayashi, M., Tamaoka, J., and Kato, C. (1998). *Pyrococcus horikoshii* sp. nov., a hyperthermophilic archaeon isolated from a hydrothermal vent at the Okinawa Trough. *Extremophiles 2*, 123-130.

Gribaldo, S., and Brochier-Armanet, C. (2006). The origin and evolution of Archaea: a state of the art. *Philos Trans R Soc Lond B Biol Sci 361*, 1007-1022.

Guan, H., Li, P., Imparl-Radosevich, J., Preiss, J., and Keeling, P. (1997). Comparing the properties of *Escherichia coli* branching enzyme and maize branching enzyme. *Arch Biochem Biophys 342*, 92-98.

Guan, H.P., and Preiss, J. (1993). Differentiation of the Properties of the Branching Isozymes from Maize (Zea mays). *Plant physiology 102*, 1269-1273.

Henrissat, B., and Bairoch, A. (1996). Updating the sequence-based classification of glycosyl hydrolases. *Biochem J 316 (Pt 2)*, 695-696.

Ho, S.N., Hunt, H.D., Horton, R.M., Pullen, J.K., and Pease, L.R. (1989). Site-directed mutagenesis by overlap extension using the polymerase chain reaction. *Gene 77*, 51-59.

Janecek, S., and Kuchtova, A. (2012). In silico identification of catalytic residues and domain fold of the family GH119 sharing the catalytic machinery with the alpha-amylase family GH57. *FEBS Le*tt *586*, 3360-3366.

Jo, H.J., Park, S., Jeong, H.G., Kim, J.W., and Park, J.T. (2015a). *Vibrio vulnificus* glycogen branching enzyme preferentially transfers very short chains: N1 domain determines the chain length transferred. *FEBS* Lett *589*, 1089-1094.

Jo, I., Chung, I.Y., Bae, H.W., Kim, J.S., Song, S., Cho, Y.H., and Ha, N.C. (2015b). Structural details of the OxyR peroxide-sensing mechanism. *Proc Natl Acad Sci U S A 112*, 6443-6448.

Kawarabayasi, Y., Sawada, M., Horikawa, H., Haikawa, Y., Hino, Y., Yamamoto, S., Sekine, M., Baba, S., Kosugi, H., Hosoyama, A., et al. (1998). Complete sequence and gene organization of the genome of a hyper-thermophilic archaebacterium, *Pyrococcus horikoshii* OT3. *DNA Res 5*, 55-76.

MacGregor, E.A., Janecek, S., and Svensson, B. (2001). Relationship of sequence and structure to specificity in the alpha-amylase family of enzymes. *Biochim Biophys Acta 1546*, 1-20.

MacGregor, E.A., and Svensson, B. (1989). A super-secondary structure predicted to be common to several alpha-1,4-D-glucan-cleaving enzymes. *Biochem J 259*, 145-152.

Murakami, T., Kanai, T., Takata, H., Kuriki, T., and Imanaka, T. (2006). A novel branching enzyme of the GH-57 family in the hyperthermophilic archaeon *Thermococcus kodakaraensis* KOD1. *J Bacteriol 188*, 5915-5924.

Otwinowski, Z., and Minor, W. (1997). Processing of X-ray diffraction data collected in oscillation mode. *Method Enzymol 276*, 307-326.

Pal, K., Kumar, S., Sharma, S., Garg, S.K., Alam, M.S., Xu, H.E., Agrawal, P., and Swaminathan, K. (2010). Crystal structure of full-length

Mycobacterium tuberculosis H37Rv glycogen branching enzyme: insights of N-terminal beta-sandwich in substrate specificity and enzymatic activity. *J Biol Chem 285*, 20897-20903.

Palomo, M., Pijning, T., Booiman, T., Dobruchowska, J.M., van der Vlist, J., Kralj, S., Planas, A., Loos, K., Kamerling, J.P., Dijkstra, B.W., et al. (2011). *Thermus thermophilus* glycoside hydrolase family 57 branching enzyme: crystal structure, mechanism of action, and products formed. *J Biol Chem 286*, 3520-3530.

Preiss, J. (2009). Glycogen: Biosynthesis and Regulation. *EcoSal Plus 3*.

Rothschild, L.J., and Mancinelli, R.L. (2001). Life in extreme environments. *Nature 409*, 1092-1101.

Santos, C.R., Tonoli, C.C., Trindade, D.M., Betzel, C., Takata, H., Kuriki, T., Kanai, T., Imanaka, T., Arni, R.K., and Murakami, M.T. (2011). Structural basis for branching-enzyme activity of glycoside hydrolase family 57: structure and stability studies of a novel branching enzyme from the hyperthermophilic archaeon *Thermococcus kodakaraensis* KOD1. *Proteins 79*, 547-557.

Seibold, G.M., Breitinger, K.J., Kempkes, R., Both, L., Kramer, M., Dempf, S., and Eikmanns, B.J. (2011). The glgB-encoded glycogen branching enzyme is essential for glycogen accumulation in *Corynebacterium glutamicum*. *Microbiology 157*, 3243-3251.

Synowiecki, J., Grzybowska, B., and Zdzieblo, A. (2006). Sources, properties and suitability of new thermostable enzymes in food processing. *Crit Rev Food Sci Nutr 46*, 197-205.

Takata, H., Takaha, T., Okada, S., Hizukuri, S., Takagi, M., and Imanaka, T. (1996a). Structure of the cyclic glucan produced from amylopectin by *Bacillus stearothermophilus* branching enzyme. *Carbohydrate research 295*, 91-101.

Takata, H., Takaha, T., Okada, S., Takagi, M., and Imanaka, T. (1996b). Cyclization reaction catalyzed by branching enzyme. *Journal of bacteriology 178*, 1600-1606.

Theriot, C.M., Semcer, R.L., Shah, S.S., and Grunden, A.M. (2011). Improving the catalytic activity of hyperthermophilic *Pyrococcus horikoshii* prolidase for detoxification of organophosphorus nerve agents over a broad range of temperatures. *Archaea 2011*, 565127.

Tormo, J., Lamed, R., Chirino, A.J., Morag, E., Bayer, E.A., Shoham, Y., and Steitz, T.A. (1996). Crystal structure of a bacterial family-III cellulose-binding domain: a general mechanism for attachment to cellulose. *EMBO J 15*, 5739-5751.

Ugalde, J.E., Parodi, A.J., and Ugalde, R.A. (2003). De novo synthesis of bacterial glycogen: Agrobacterium tumefaciens glycogen synthase is involved in glucan initiation and elongation. *Proc Natl Acad Sci U S A 100*, 10659-10663.

Wang, L., and Wise, M.J. (2011). Glycogen with short average chain length enhances bacterial durability. *Naturwissenschaften 98*, 719-729.

Watanabe, H., Nishimoto, T., Kubota, M., Chaen, H., and Fukuda, S. (2006). Cloning, sequencing, and expression of the genes encoding an isocyclomaltooligosaccharide glucanotransferase and an alpha-amylase from a *Bacillus circulans* strain. *Biosci Biotechnol Biochem 70*, 2690-2702.

Zona, R., Chang-Pi-Hin, F., O'Donohue, M.J., and Janecek, S. (2004). Bioinformatics of the glycoside hydrolase family 57 and identification of catalytic residues in amylopullulanase from *Thermococcus hydrothermalis*. *Eur J Biochem 271*, 2863-2872.

VI. 국문초록

글리코젠 분지 효소 (glycogen branching enzyme; GBE)는 알파-1,4 글리코시딕 결합을 절단하는 가수분해 활성과, 알파-1,6 글리코시딕 결합을 형성하는 글리코실 전이 활성 (transglycosylation)을 갖는 효소로, 글리코겐 생성 과정의 마지막 단계에서 알파-1,6 분지점 형성을 촉매하는 역할을 하게 된다. 대부분의 분지 효소는 글리코시드 가수분해효소군 13 (glycoside hydrolase family 13; GH13)에 속하지만, 최근 연구 결과에 따르면 몇몇 고세균 유래 분지효소가 새로이 글리코시드 가수분해효소군 57 (glycoside hydrolase family 57; GH57)에 속하는 것으로 밝혀졌다. 본 연구에서는 고호열성 고세균인 *Pyrococcus horikoshii* 에서 유래한 GH57 그룹에 속하는 분지 효소의 결정 구조를 2.3 Å 의 해상도로 규명하였다. 이 분지 효소는 세 개의 서로 다른 도메인으로 이루어져 있다. 중심에 위치한 $(\beta/\alpha)_7$ 배럴 도메인과 다섯 개의 알파 나선 구조로 이루어진 C- 말단 도메인, 그리고 그 가운데에 세 개의 알파 나선 구조로 이루어진 도메인으로 구성되어 있다. 활성 부위는 중앙 도메인과 C- 말단 도메인의 접점 (interface)에 위치한다. 글리코젠 산물의 가지 길이에 영향을 미칠 것으로 예상되는 트립토판 (tryptophan) 잔기를 알라닌 (alanine)으로 치환한 점

돌연변이 단백질의 경우에는 분지 효소의 두 가지 활성이 모두 사라지는 것을 확인할 수 있었다. 이 결과를 토대로 트립토판 잔기가 위치한 곳이 기질이 결합하는 곳이라는 점과 트립토판 잔기가 분지 효소와 기질 간의 상호작용에 있어서 중요한 역할을 하고 있음을 확인할 수 있었다. 또한, 활성 잔기들과 상호작용을 하는 것으로 예상되는 루프를 제거한 돌연변이 단백질에서는 가수 분해 활성이 증가하고 최종 산물의 가지 길이가 변하는 결과를 보였다. 이러한 결과들을 종합하여 GH57 그룹에 속하는 분지 효소의 두 가지 활성과 기질과의 상호작용에 관한 분자적인 작용 메커니즘을 제시할 수 있었다. 나아가 본 연구를 통해, 구조를 기반으로 분지 효소의 산물인 글리코젠의 가지 길이를 변화시킴으로써 산업적으로 기능성 식품 산업에서 이용할 수 있을 것으로 기대된다.

주요어: X 선 결정학, *Pyrococcus horikoshii*, 글리코젠, 아밀로스, 분지 효소

학번: 2015-21770